Zahn, R., Comas, M.C., and Klaus, A. (Eds.), 1999
Proceedings of the Ocean Drilling Program, Scientific Results, Vol. 161

28. *DATA REPORT:* MAJOR- AND TRACE-ELEMENT CHEMISTRY OF SITE 976 BASEMENT ROCKS (ALBORAN SEA)[1]

P. Spadea[2] and G. Prosser[3]

INTRODUCTION

At Site 976, the Alboran Sea basement was cored between 669.73 mbsf and 928.7 mbsf at Hole 976B, and between 652.08 mbsf and 736.3 mbsf at Hole 976E. The total recovery of basement rock was 50.4 m at Hole 976B and 24.74 m at Hole 976E (Shipboard Scientific Party, 1996). In both holes the lithotype sequence includes dominant high-grade metasedimentary rocks, metapelitic schist and paragneiss, marble and calc-silicate rock, and minor leucogranite. The rocks display a complicated history of metamorphism and deformation, which is relevant for the geodynamic interpretation of the Alboran Sea (C. Doglioni, E. Gueguen, F. Sabat, and M. Fernandez, unpubl. data; G. Prosser, P. Spadea, and C. Doglioni, unpubl. data).

Major- and trace-element analysis on representative samples of basement rock from Holes 976B and 976E were performed in order to provide useful data to: (1) characterize the sedimentary protoliths, (2) evaluate partial melting processes, and (3) compare the drilled Alboran Sea basement with basement exposed on-land at the Betic Cordillera. Analyzed lithotypes include high-grade schist, banded paragneiss and leucocratic gneiss, a banded schist/calc-silicate rock, and a leucosome interlayered within high-grade schist (Table 1).

ANALYTICAL TECHNIQUES

Whole-rock X-ray fluorescence (XRF) analyses were made on the Philips PW1400 spectrometer at Udine University (analyst P. Ciet). Major elements, Sc and Cr were measured on lithium borate glass disks prepared with flux to sample ratio of 10:1 to reduce matrix effects. The trace elements V, Ni, Cu, Zn, Rb, Y, Sr, Zr, Nb, and Ba were determined on powder pellets adopting Compton scattering technique for matrix absorption correction. For trace elements, the analytical precision was better than 2%–10% (2sd). Loss on ignition was determined by the gravimetric method. Rare earth elements (REE) were separated using conventional ion-exchange chromatographic techniques after leaching in hot $HClO_4$ + HF. Eventual insoluble residuum was fused with $LiBO_2$ and leached similarly. REE analyses were made on the Jobin-Yvon JY38 inductively coupled plasma spectrometer at Udine University (analyst P. Ciet). The analytical precision was better than 5% (2sd).

RESULTS AND DISCUSSION

The results of major- and trace-element analyses are listed in Table 2. Firstly, major oxides data are compared, and commented on with respect to the chemical characterization of the sedimentary protoliths. The high-grade schists (petrologic group 1) are rich in K_2O relative to Na_2O, and show large variations in SiO_2 (59–72 wt%) and Al_2O_3 content (13–22 wt%). Al_2O_3 and TiO_2 are negatively correlated with SiO_2, whereas the other major oxides are variable and mostly unrelated to SiO_2 variations. The chemistry of the banded schist-calc-silicate rock (petrologic group 1a) compared with the high-grade schists, shows clear chemical evidence of the dilution effect of a carbonate component. The two analyzed samples from petrologic group 2 (gneiss and migmatitic gneiss) are notably different, particularly in Al_2O_3 and CaO contents, the migmatitic gneiss being chemically close to the petrologic group 1 schists. The quartz- and feldspar-rich gneisses of petrologic group 3 are also not homogeneous chemically and have distinctive high SiO_2 and low Al_2O_3 with respect to the petrologic group 2 gneisses. The analyzed leucosome (Sample 161-976B-98R-2, 48–50 cm) is close to a granitic composition in terms of major components. However, as commented below, the contents of compatible trace elements Ni and Cr appear in excess for a normal granite composition, thus suggesting that the rock is not purely magmatic, but includes a significant component from the sedimentary protolith. This sample is therefore included with the metasedimentary ones for subsequent chemical characterizations.

To investigate the nature of the sedimentary protoliths according to the major oxide contents, the discriminant diagram ACF (Winkler, 1979) and variation diagrams of oxide vs. Al_2O_3 have been selected and are shown in Figures 1 and 2. The average shale PAAS (post-Archean Australian Shale) calculated by Taylor and MacLennan (1985) has been used as reference composition for dominantly terrigenous sediments according to Plank and Ludden (1992). Data plotted in the ACF diagram (Fig. 1) indicate that most high-grade schists and the migmatitic gneiss are metapelites close to PAAS, except one schist, which is higher in the A component. Two gneisses (a banded gneiss and a felsic gneiss) are plotted similarly in the graywacke field. Variation diagrams (Fig. 2) also show the similarities of the high-grade schists (petrologic group 1) and the banded gneiss from petrologic group 2 with PAAS, while clearly distinguishing the felsic gneisses and leucosome (petrologic group 3) from the metapelites.

Further characterization of the protoliths is obtained from trace elements, particularly from REEs. In variation diagrams against Al_2O_3 (Fig. 2), the REE Sm and Cr have been selected to compare the analyzed samples and refer them to PAAS. Plots show that Sm correlates with Al_2O_3 similarly to TiO_2, but is significantly higher than in PAAS. Cr is comparable to PAAS and dispersed similarly to Fe_2O_3 + MgO.

The REEs appear to provide the best information on primary composition, and also give some insight on metamorphic differentiation and/or melting processes. Chondrite-normalized REEs patterns of the petrologic groups are shown in Figure 3. For high-grade schists, REEs are remarkably consistent, showing strongly L (light) REE enriched, parallel patterns, without significant Ce anomaly and with a marked Eu anomaly. The banded schist-calc-silicate rock (Sample 161-976B-16R1, 106–110 cm) is distinct from the high-grade schists for a lower enrichment of LREE and a marked enrichment of H (heavy) REE with respect to M (middle) REE, clearly reflecting the composition of the carbonate component. The two gneisses of petrologic group 2 display similar patterns and are close to those of the high-grade schists. In terms of REE patterns, the felsic gneisses and leucosome of petrologic group 3 are clearly distinguished from each other and from the other petrologic groups. In particular the felsic

[1]Zahn, R., Comas, M.C., and Klaus, A. (Eds.), 1999. *Proc. ODP, Sci. Results,* 161: College Station, TX (Ocean Drilling Program).
[2]Dept. GEOTER, University of Udine, Via Cotonificio 114, I-33100 Udine, Italy. spadea@dgt.uniud.it
[3]Centro di Geodinamica, University of Basilicata, Via Anzio, I-85100 Potenza, Italy.

Table 1. Petrography of the basement samples analyzed from Site 976.

Core, section, interval (cm)	Rock type	Petrologic group
161-976B-		
76R-1, 93-97	Bt Amp schist	1: High-grade schist (metapelite)
83R-2, 94-98	Bt-Sil-And-Pl-Kfs schist	1: High-grade schist (metapelite)
95R-1, 25-29	Bt gneiss (quartz-rich)	3: Felsic gneiss and leucosome
96R-1, 35-39	Bt-Ms-Sil-And-Crd-Pl-Kfs migmatitic gneiss	2: Banded gneiss and migmatitic gneiss
98R-2, 48-50	Qtz-Crd-Kfs-Ms-And-Bt leucosome	3: Felsic gneiss and leucosome
101R-1, 19-21	Banded gneiss with Amp-Crd-, Bt-, and Pl-Kfs-And layers	2: Banded gneiss and migmatitic gneiss
106R-1, 94-97	And-Sil-Crd-Fd-Bt gneiss (quartz-rich)	3: Felsic gneiss and leucosome
161-976E-		
16R-1, 106-110	Interlayered Bt-Amp schist and Spl-Px calc-schist	1a: High-grade schist and calc-silicate rock
19R-1, 4-8	Bt-Sil-Pl-Kfs schist	1: High-grade schist (metapelite)
21R-1, 134-139	Pl-Bt-Sil-Tur schist	1: High-grade schist (metapelite)
22R-1, 120-122	Pl-Bt-Grt schist	1: High-grade schist (metapelite)

Note: Bt = biotite, Amp = amphibole, Sil = sillimanite, And = andalusite, Pl = plagioclase, Kfs = potash feldspar, Ms = muscovite, Crd = cordierite, Qtz = quartz, Spl = spinel, Px = pyroxene, Tur = tourmaline, Grt = garnet.

Table 2. Major- and trace-element analyses of representative basement samples from Site 976.

Hole:	976B	976B	976B	976B	976B	976B	976B	976E	976E	976E	976E
Core, section, Interval (cm):	76R-1, 93-97	83R-2, 94-98	95R-1, 25-29	96R-1, 35-39	98R-2, 48-50	101R-1, 19-21	106R-1, 94-97	16R-1, 106-110	19R-1, 4-8	21R-1, 134-139	22R-1, 120-122
Petrologic group:	1	1	3	2	3	2	3	1a	1	1	1
SiO_2	59.70	62.75	77.36	55.09	74.16	54.45	74.11	58.82	61.88	59.40	72.80
TiO_2	0.90	0.98	0.70	1.00	0.46	0.85	0.87	0.82	1.10	1.11	0.73
Al_2O_3	16.60	19.00	10.67	23.16	14.51	19.46	13.26	18.05	21.99	21.86	12.92
Fe_2O_3	7.26	7.58	4.09	8.77	3.03	10.23	4.74	4.41	8.28	8.30	6.59
MnO	0.19	0.06	0.12	0.07	0.05	0.18	0.03	0.05	0.07	0.08	0.11
MgO	4.67	1.85	2.00	2.15	1.07	4.28	1.01	1.59	1.74	1.80	2.10
CaO	7.63	2.12	3.03	2.58	1.77	7.02	1.68	13.60	0.57	2.30	1.47
Na_2O	0.40	1.53	0.41	2.26	1.66	1.10	2.15	0.81	0.45	1.01	0.65
K_2O	2.25	3.62	1.30	4.44	3.09	1.98	1.84	1.38	3.68	3.67	2.30
P_2O_5	0.14	0.18	0.11	0.18	0.15	0.19	0.09	0.22	0.18	0.17	0.13
Total	99.74	99.67	99.79	99.70	99.95	99.74	99.78	99.75	99.94	99.70	99.80
LOI	1.81	3.79	2.33	3.17	3.73	2.73	2.24	11.94	7.10	4.94	4.60
Sc	21	24	10	25	5	21	11	23	22	24	15
V	103	151	57	153	58	131	83	160	165	164	108
Cr	123	110	67	124	58	113	76	139	126	116	101
Ni	57	38	23	54	15	64	31	62	44	60	45
Cu	14	27	5	5	16	11	8	25	5	14	18
Zn	86	112	45	104	46	120	56	77	105	108	58
Rb	139	167	96	191	115	150	73	76	169	190	118
Sr	185	346	121	244	182	216	207	329	220	304	148
Y	45	33	30	33	22	28	29	44	33	34	31
Zr	428	202	323	185	123	223	289	145	182	196	197
Nb	22	14	14	17	9	20	14	15	17	16	14
Ba	343	428	331	951	715	113	751	207	427	379	347
La	51.0	39.5	27.6	50.0	20.2	46.0	34.0	32.5	45.4	48.3	22.5
Ce	104.0	82.2	56.6	103.0	41.4	93.0	68.0	67.4	97.0	100.0	45.5
Nd	43.0	33.6	21.9	43.0	17.3	39.0	29.0	28.4	39.0	42.0	18.6
Sm	9.40	8.70	4.77	9.10	3.90	8.67	5.97	6.20	8.07	8.94	4.42
Eu	1.63	1.53	0.93	1.84	0.93	1.51	1.17	1.26	1.34	1.54	0.69
Gd	8.10	5.79	3.99	6.86	3.42	6.86	5.00	5.34	6.35	6.89	4.57
Dy	6.90	5.21	2.61	5.54	3.32	4.83	4.44	5.91	5.48	5.94	5.04
Er	3.70	2.83	0.86	2.95	1.84	2.34	2.34	4.27	3.00	3.35	3.13
Yb	3.47	2.83	0.68	2.83	1.88	2.52	2.25	4.69	2.94	3.27	3.27
Lu	0.52	0.45	0.10	0.44	0.30	0.42	0.34	0.69	0.46	0.51	0.51

Note: Major elements reported in wt%; trace elements are in ppm.

gneiss Sample 161-976B-106R-1, 94–97 cm, has higher and more LREE-enriched REE contents than the leucosome Sample 161-976B-98R-2, 48–50 cm. The felsic gneiss Sample 161-976B-95R-1, 25–29 cm, has a unique REE pattern, displaying a marked HREE depletion suggesting that HREE were fractionated by garnet crystallization in adjacent mafic or restitic bands.

The PAAS-normalized REE values shown in Figure 3, give some indications similar to the chondrite/normalized values, but also evidence markedly variable patterns of the high-grade schists and emphasize the difference between the two gneisses of group 2. For the felsic gneiss Sample 161-976B-95R-1, 25–29 cm, the marked HREE depletion is also evidenced. In general, the similarity of the high-grade schists and gneisses to average shale is confirmed, and dilution effects by silica are also displayed by the high-grade schists.

Finally, a synthesis of the chemical characteristics of the analyzed samples is presented in Figure 4 as PAAS-normalized abundances of elements in order of increasing compatibility in melting processes (Pearce and Parkinson, 1993).

REFERENCES

Nakamura, N., 1974. Determination of REE, Ba, Fe, Mg, Na, and K in carbonaceous and ordinary chondrites. *Geochim. Cosmochim. Acta,* 38:757–776.

Pearce, J.A., and Parkinson, I.J., 1993. Trace element models for mantle melting: application to volcanic arc petrogenesis. *In* Pritchard, H.M., Alabaster, T., Harris, N.B.W., and Neary, C.R. (Eds.), *Magmatic Processes and Plate Tectonics.* Geol. Soc. Spec. Publ. London, 76:373–403.

Plank, T., and Ludden, J.N., 1992. Geochemistry of sediments in the Argo Abyssal Plain at Site 765: a continental margin reference section for sediment recycling in subduction zones. *In* Gradstein, F.M., Ludden, J.N., et al., *Proc. ODP, Sci. Results,* 123: College Station, TX (Ocean Drilling Program), 167–189.

Shipboard Scientific Party, 1996. Site 976. *In* Comas, M.C., Zahn, R., Klaus, A., et al., *Proc. ODP, Init. Repts.,* 161: College Station, TX (Ocean Drilling Program), 179–297.

Taylor, S.R., and McLennan, S.M., 1985. *The Continental Crust: Its Composition and Evolution:* Oxford (Blackwell Scientific).

Winkler, H.G.F., 1979. *Petrogenesis of Metamorphic Rocks:* New York (Springer-Verlag).

Date of initial receipt: 9 May 1997
Date of acceptance: 6 November 1997
Ms 161SR-272

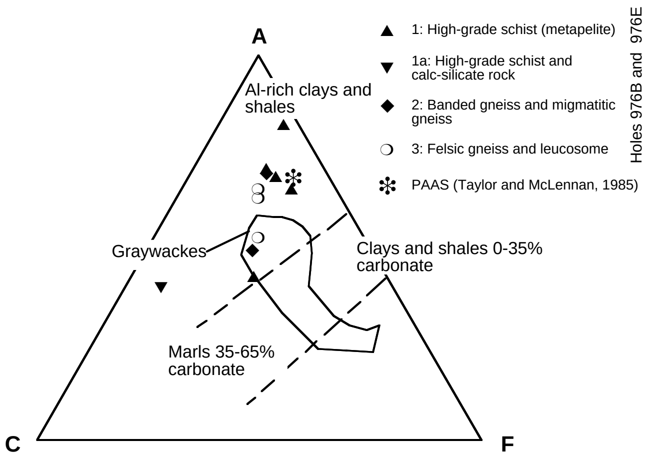

Figure 1. Projections in the ACF diagram (Winkler, 1979) of the Alboran Sea basement samples analyzed.

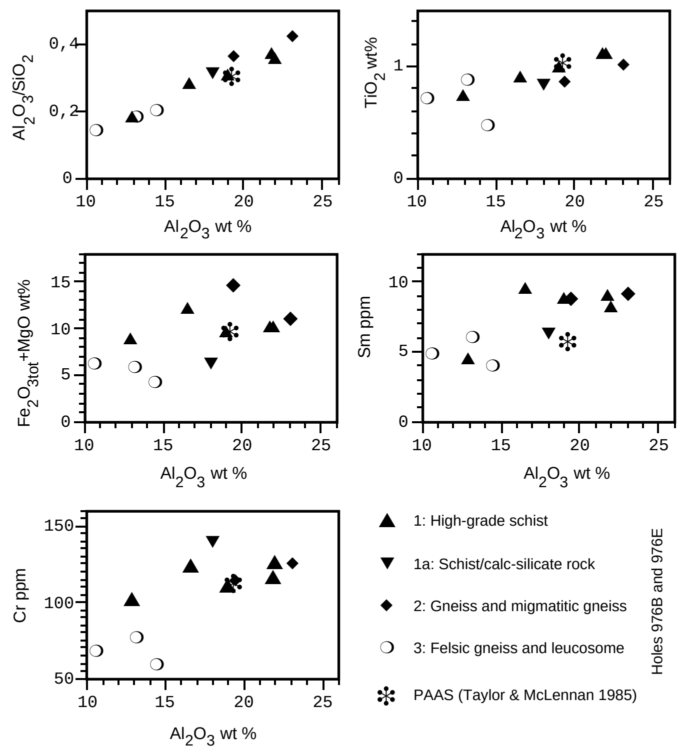

Figure 2. Variations of Al_2O_3/SiO_2, TiO_2, Fe_2O_3 + MgO and trace elements Cr and Sm vs. Al_2O_3 and comparison with average shale (PAAS: data from Taylor and MacLennan, 1985).

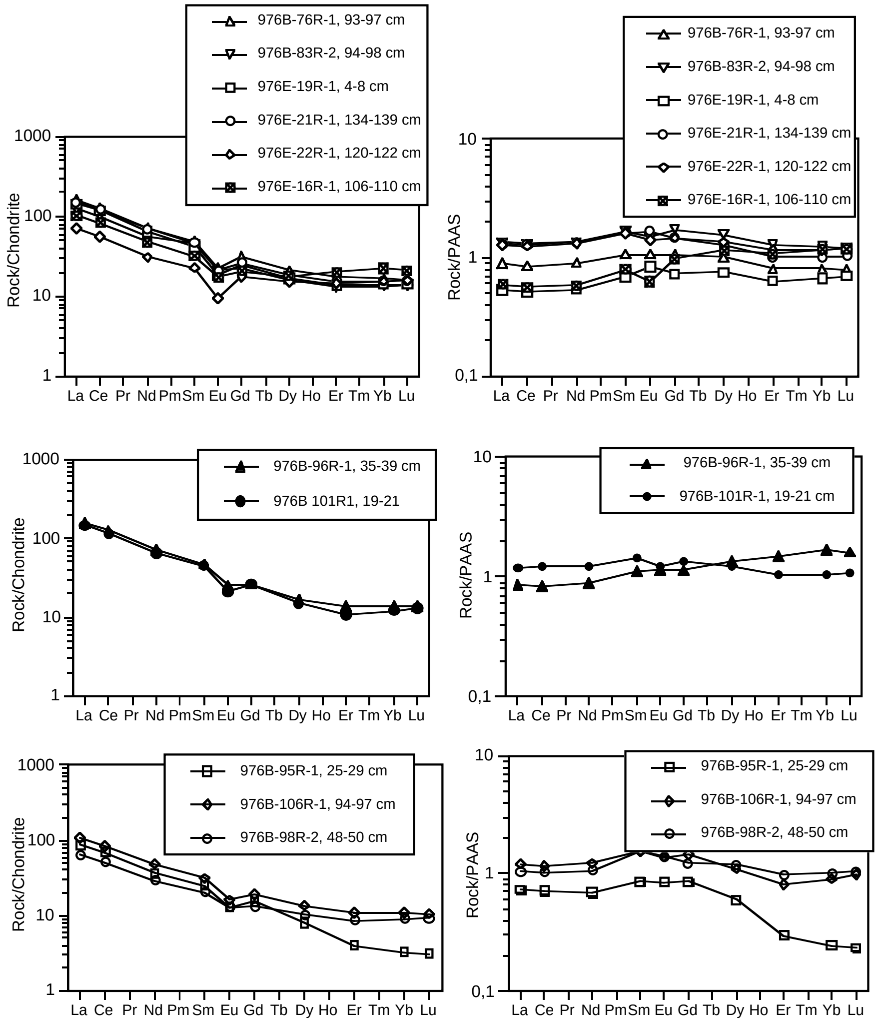

Figure 3. Chondrite-normalized and PAAS-normalized REE patterns for the Alboran Sea basement samples analyzed. Chondrite normalization values from Nakamura (1974); PAAS normalization values from Taylor and MacLennan (1985).

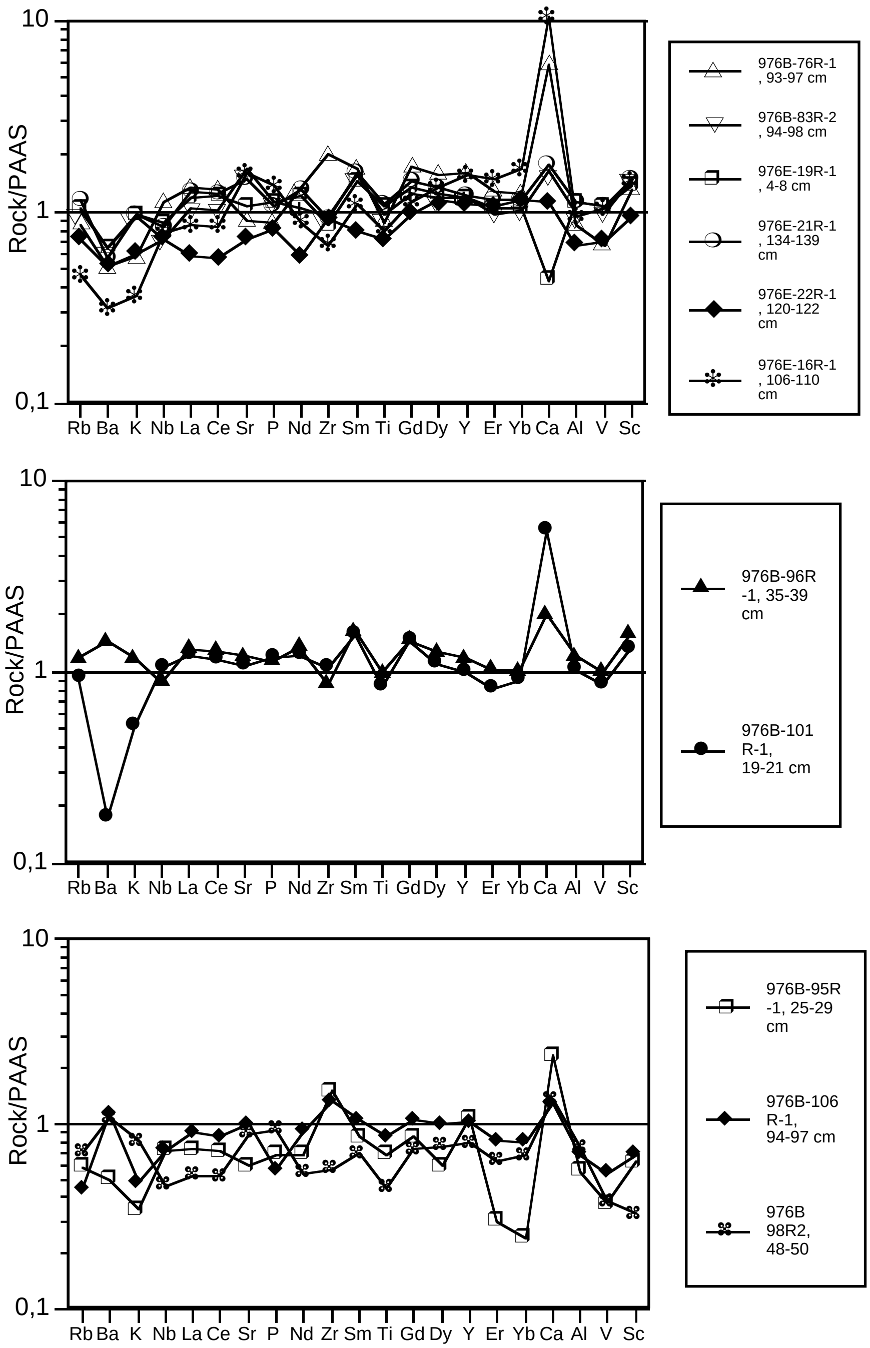

Figure 4. PAAS-normalized spider diagram for the Alboran Sea basement samples analyzed. Elements are in order of increasing compatibility; PAAS values are taken from Taylor and MacLennan (1985).